

Article

Effect of Fine Particle Peening Using Hydroxyapatite Particles on Rotating Bending Fatigue Properties of β -Type Titanium Alloy [†]

Yuki Nakamura ^{1,*}, Koichiro Nambu ², Toshikazu Akahori ³, Toshihiro Shimizu ¹ and Shoichi Kikuchi ⁴ 

¹ Department of Mechanical Engineering, National Institute of Technology, Toyota College, Toyota 471-8525, Japan; shimizu@toyota-ct.ac.jp

² Faculty of Engineering, Osaka Sangyo University, Daito 574-8530, Japan; knambu.mech@ge.osaka-sandai.ac.jp

³ Faculty of Science and Technology, Meijo University, Nagoya 468-8502, Japan; akahori@meijo-u.ac.jp

⁴ Faculty of Engineering, Shizuoka University, Hamamatsu 432-8561, Japan; kikuchi.shoichi@shizuoka.ac.jp

* Correspondence: nakamura@toyota-ct.ac.jp

[†] This paper is an extended version of our paper published in Proceedings of the 13th World Conference on Titanium.

Abstract: Fine particle peening (FPP) using hydroxyapatite (HAp) shot particles was performed to improve the fatigue strength and form a HAp transfer layer on a beta titanium alloy (Ti-22V-4Al). The surface microstructures of the FPP-treated specimen were characterized using scanning electron microscopy, micro-Vickers hardness testing, energy dispersive X-ray spectrometry, X-ray diffraction, and electron backscattered diffraction. A HAp transfer layer with a thickness of 5.5 μm was formed on the surface of the Ti-22V-4Al specimen by FPP. In addition, the surface hardness of the Ti-22V-4Al was increased, and high compressive residual stress was generated on the specimen surface by FPP. Rotating bending fatigue tests were performed at room temperature in laboratory air over a wide cycle-life region (10^3 – 10^9 cycles). In the long cycle-life regime, the fatigue strength at 10^7 cycles of the FPP-treated specimen became higher than that of the untreated specimen. This result is attributed to the formation of a work-hardened layer with high compressive residual stress by FPP. However, the fatigue strength was not improved by FPP in the short cycle-life regime, because fatigue cracks were initiated at surface defects formed during the FPP process. The fatigue fracture mode of the FPP-treated specimens shifted from surface-initiated fracture to subsurface-initiated fracture at a stress amplitude level of 600 MPa.

Keywords: fine particle peening; hydroxyapatite; beta titanium alloy; rotating bending; very high cycle fatigue



Citation: Nakamura, Y.; Nambu, K.; Akahori, T.; Shimizu, T.; Kikuchi, S. Effect of Fine Particle Peening Using Hydroxyapatite Particles on Rotating Bending Fatigue Properties of β -Type Titanium Alloy. *Appl. Sci.* **2021**, *11*, 4307. <https://doi.org/10.3390/app11094307>

Academic Editor: Massimo Rossetto

Received: 31 March 2021

Accepted: 7 May 2021

Published: 10 May 2021

Publisher's Note: MDPI stays neutral with regard to jurisdictional claims in published maps and institutional affiliations.



Copyright: © 2021 by the authors. Licensee MDPI, Basel, Switzerland. This article is an open access article distributed under the terms and conditions of the Creative Commons Attribution (CC BY) license (<https://creativecommons.org/licenses/by/4.0/>).

1. Introduction

Titanium alloys are used for implant components [1] because of their high corrosion resistance, high specific strength, lower Young's modulus than ferrous materials, and so on. In recent years, requirements for the safety of implant components have become increasingly stringent; therefore, the fatigue behavior of titanium alloys has become a priority in fatigue research. In particular, research clarifying the fatigue properties in the very high cycle regime, such as 10^8 – 10^{10} cycles, is very important to secure the long-term reliability of implant components. However, research on the very high cycle fatigue behavior of titanium alloys is relatively scarce, compared with that on ferrous metals. Some researchers have reported that fatigue failure occurred even in the very high cycle regime for titanium alloys, such as Ti-6Al-4V [2–4], Ti-8Al-1Mo-1V [5], Ti-5Al-2Sn-2Zr [6], and VT3-1 [7].

The β -type titanium alloy used in this study possesses better cold workability than other titanium alloys. Thus, it is easier to machine into complicated shapes than other

titanium alloys. Furthermore, heat treatment gives β -type titanium alloys high static strength. These material properties enable β -type titanium alloys to be used to make individualized implant components with high strength.

Surface modification processes have been introduced to provide good biological compatibility and strong bonding between bone structures and titanium alloys using hydroxyapatite (HAp) coatings. One modification of the HAp coating process has been introduced for the $\alpha + \beta$ titanium alloy Ti-6Al-4V [8,9] and commercially pure titanium (CP titanium) [10,11]. However, it has been reported that fatigue fracture often occurs at the interface between the HAp coating layer and the substrate under cyclic loading [11]. Furthermore, thermal energy induced by high-temperature processes, such as plasma spraying, changes the crystalline structure of HAp [12] or the titanium substrate, [13] and this phenomenon has a negative effect on HAp-coated bio-implants.

Based on this background, it is important to create a HAp coating layer without changing the crystalline structure of HAp. In recent years, it has been reported that FPP treatment can form a surface-modified layer enriched with the colliding particles of carbon steel [14], titanium [15], chromium [16], and carbon-black/steel [17] at room temperature. In our previous studies [18–20], a HAp transfer layer was formed by FPP using HAp particles on CP titanium, Ti-6Al-4V alloy, and Ti-29Nb-13Ta-4.6Zr alloy without any change in the crystalline structure of HAp. Furthermore, FPP can modify the microstructure and the fatigue strength of metallic materials [21–24]; the fatigue strength of CP titanium and the fatigue life of Ti-6Al-4V were improved by FPP.

In the present study, FPP using HAp particles was used to form a HAp transfer layer and improve the fatigue strength of a beta titanium alloy (Ti-22V-4Al). The purpose of this study was to characterize the FPP transfer layer and to experimentally examine the effect of FPP using HAp particles on the fatigue properties of the Ti-22V-4Al alloy under rotating bending. Furthermore, fatigue fracture mechanisms were identified by fractography using SEM. The effect of FPP using HAp particles on fatigue behavior was discussed in light of the fractography results.

2. Experimental Procedures

2.1. Material and Specimens

The material used in this study was a beta titanium alloy (Ti-22V-4Al) provided by a research subcommittee on very high cycle fatigue in the Society of Materials Science, Japan (JSMS). The chemical composition (mass%) of the material is Al: 4.15, V: 21.17, Fe: 0.15, C: 0.013, O: 0.14, N: 0.012, H: 0.0124, Ti: bal. This material was given a solution treatment (1023 K, 3.6 ks, water quenching) and aging treatment (823 K, 14.4 ks, air cooling). The mechanical properties of the material after heat treatment are listed in Table 1. Figure 1 shows the microstructure of the material as analyzed by electron backscattered diffraction (EBSD). The acicular alpha phase was produced by the aging process at the grain boundaries of the beta phase. After the heat treatments, the material was machined to hourglass-shaped fatigue specimens, whose configuration is shown in Figure 2, and the surface on the center notch of the specimens was finished by buffing to a mirror finish after polishing with #400–#4000 emery papers in the axial direction of the specimen.

Table 1. Mechanical properties of Ti-22V-4Al alloy.

Young's Modulus E (GPa)	Yield Stress σ_Y (MPa)	Tensile Strength σ_{UT} (MPa)	Elongation δ (%)	Reduction of Area φ (%)	Vickers Hardness HV
97	1154	1235	9.3	21.9	261

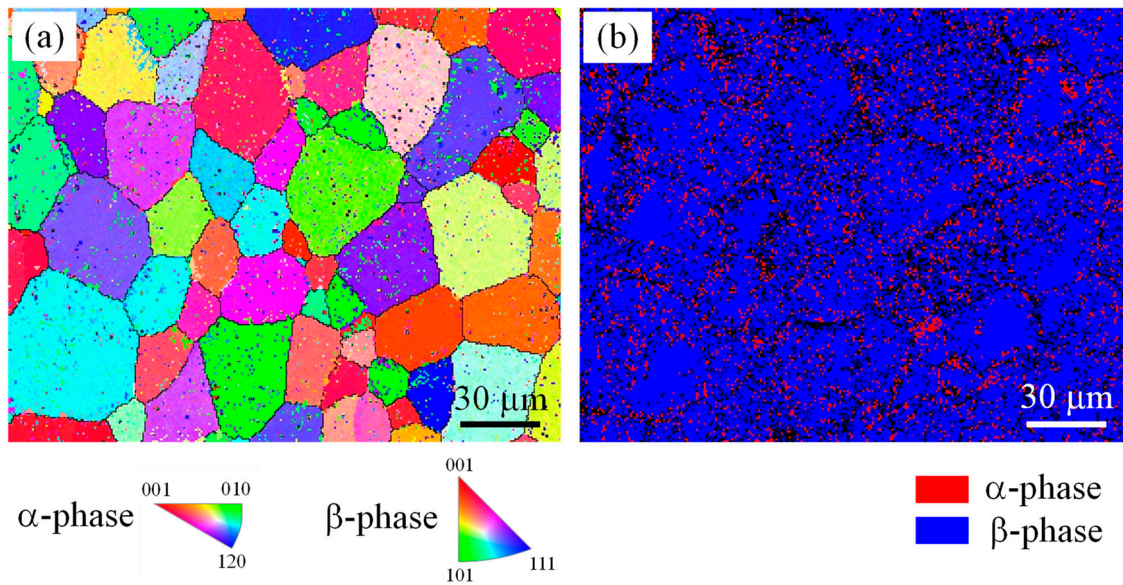


Figure 1. EBSD analysis of microstructure: (a) inverse pole figure (IPF) map; (b) phase map.

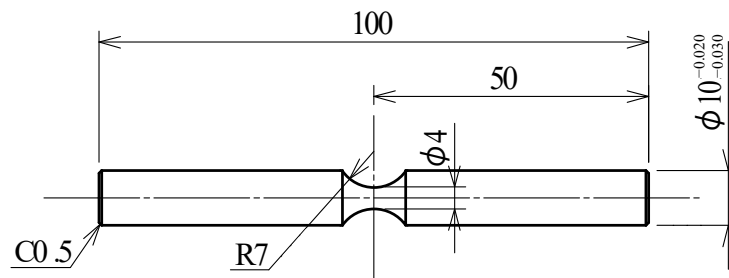


Figure 2. Specimen configuration.

FPP treatment was conducted at room temperature in ambient air with a peening pressure of 0.6 MPa and a peening time of 30 s on the polished specimen surface. The distance between the specimen surface and the tip of the nozzle was 50 mm. The shot particles, with a diameter of 50 μm , were produced by pulverizing HAp ($\text{Ca}_{10}(\text{PO}_4)_6(\text{OH})_2$) fabricated by Eccera Co., Ltd.

Before the fatigue test, the FPP-treated specimens were placed in acetone in an ultrasonic bath to remove the free HAp particles on the specimen surface.

2.2. Characterization of FPP-Treated Surface

The surface microstructure of the specimens was characterized using scanning electron microscopy (SEM). An FPP-treated specimen was also analyzed using energy dispersive X-ray spectroscopy (EDS). The cross section perpendicular to the axial direction of the FPP-treated specimen was analyzed by EBSD. The hardness distributions were measured along the longitudinal section of the FPP-treated specimen using a micro-Vickers hardness tester with an indentation force of 0.098 N and a load holding time of 10 s. The residual stress and the full width at half maximum (FWHM) were also measured at given depths for the transverse section of the specimen by X-ray diffraction (XRD) with $\text{CuK}\alpha$ radiation. The conditions for the residual stress measurement are shown in Table 2.

Table 2. Residual stress measurement conditions.

Tube voltage, kV	40
Tube current, mA	30
Diffraction angle 2θ , deg	128
Diffraction plane	(321)
Incident angle, deg	0, 15, 22, 28, 33, 37, 41, 45
Beam diameter, mm	1.0
Stress constant, MPa/deg	−361.62

2.3. Fatigue Tests and Fracture Surface Observation

Fatigue tests were performed using a cantilever-type rotary bending fatigue testing machine. The machine has two spindles driven by an electric motor via a flat belt, and each spindle has specimen grips at both ends [25]. Thus, it can perform fatigue tests on four specimens simultaneously. The eccentricity of the specimens mounted to the specimen grips was kept within $\pm 20 \mu\text{m}$ at the tip of each specimen. The rotation speed of the spindle was 3150 rpm. All the fatigue tests were conducted at room temperature and in a laboratory environment. After fatigue tests, fracture surfaces of the failed specimens were examined by means of SEM.

3. Results and Discussion

3.1. Characterization of HAp Layer Formed by FPP

Figure 3 shows SEM micrographs and EDS maps of each specimen surface. EDS analysis was conducted with a working distance of 10 mm, an accelerating voltage of 20 kV, and a magnification of 100 for all specimens. As can be seen in the SEM micrograph of the FPP-treated specimen surface, a rough surface was formed by plastic deformation due to the collision of HAp particles with the specimen surface. As a result of measuring the surface roughness (arithmetic mean roughness, R_a , and maximum height, R_z), it was found that $R_a = 0.02 \mu\text{m}$ and $R_z = 0.16 \mu\text{m}$ for the untreated specimen, while $R_a = 0.45 \mu\text{m}$ and $R_z = 2.96 \mu\text{m}$ for the FPP-treated specimen. As a result of EDS analysis, only titanium (Ti) was detected in the untreated specimen. In contrast, calcium (Ca), oxygen (O), and phosphorus (P), which were contained in the HAp particles, were also detected over the whole surface of the FPP-treated specimen. These results suggest that a HAp transfer layer was formed on the surface of the Ti–22V–4Al alloy.

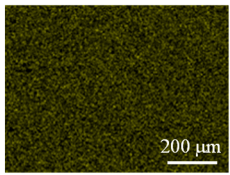
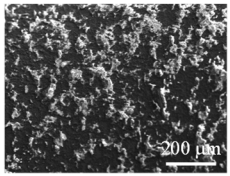
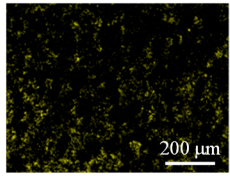
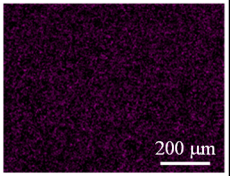
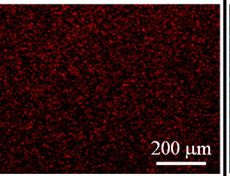
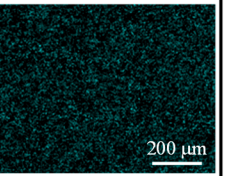
	SEM micrograph	Ti	Ca	O	P
Untreated			Not detected	Not detected	Not detected
FPP-treated					

Figure 3. SEM micrographs and EDS maps for surface of untreated specimen and FPP-treated specimen.

Figure 4 shows the elemental composition of each specimen surface analyzed by EDS. Ca, P, and O were detected and accounted for 84% of the composition of the FPP-treated

specimen surface. Therefore, the HAp was definitely transferred on the surface of the titanium alloy, because the amount of HAp constituent elements clearly increased.

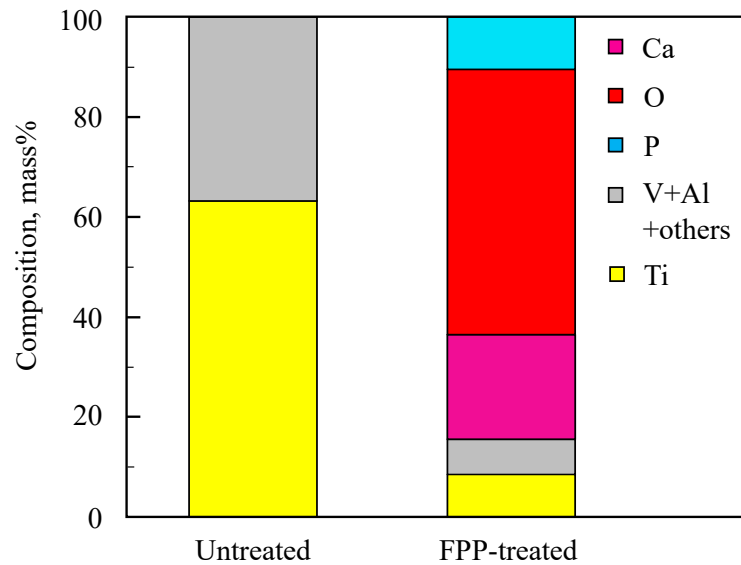


Figure 4. Elemental composition of untreated and FPP-treated specimen surface determined by EDS analysis.

To investigate the thickness of the HAp layer, we observed the cross section of an FPP-treated specimen. Figure 5 shows the cross-sectional SEM micrograph and EDS maps of the FPP-treated specimen. Ca, O, and P, which are contained in the HAp shot particles, were detected on the Ti alloy substrate. Thus, it was again confirmed that the HAp layer was formed on the Ti-22V-4Al alloy. Figure 5 also reveals that the HAp layer was inhomogeneously formed at the FPP-treated surface. The equivalent thickness of the HAp layer was calculated from Equation (1), assuming that the HAp layer, which consisted of HAp shot particles transferred onto the surface, was uniformly formed over the entire surface [23]:

$$t_{eq} = area_{Ca} / b \tag{1}$$

where t_{eq} is the equivalent thickness of the HAp layer (μm), $area_{Ca}$ is the area where calcium was detected (μm^2), and b is the width of the specimen in the analyzed area ($42.3 \mu\text{m}$). The $area_{Ca}$ and the b were calculated using image processing in the cross-sectional image of the FPP-treated specimen. As a result of the calculation, t_{eq} was $5.5 \mu\text{m}$. In our previous study, a HAp layer was formed by FPP on an $\alpha + \beta$ Ti-6Al-4Al alloy having a Vickers hardness of 340 HV [23], and the thickness was $7.0 \mu\text{m}$. There was no noticeable difference in the thickness of the HAp layer formed in the present study. This result indicates that the thickness of the HAp layer has no dependence on the Vickers hardness of the substrate in the range from 261 to 340.

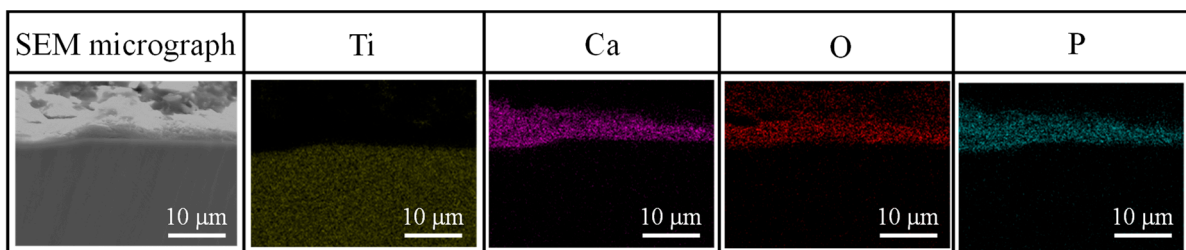


Figure 5. SEM micrographs and EDS maps for cross section of FPP-treated specimen.

3.2. Effect of FPP on the Microstructure of the Ti-22V-4Al Alloy

Figure 6 shows the image quality (IQ), inverse pole figure (IPF), and phase maps for the cross section of the FPP-treated specimen analyzed by EBSD. In Figure 6b,c, there was no noticeable difference in microstructure as compared with the microstructure of the substrate (Figure 1) even beneath the surface. Thus, no change in microstructure, such as crystal grain refinement, occurred as a result of FPP using HAp particles.

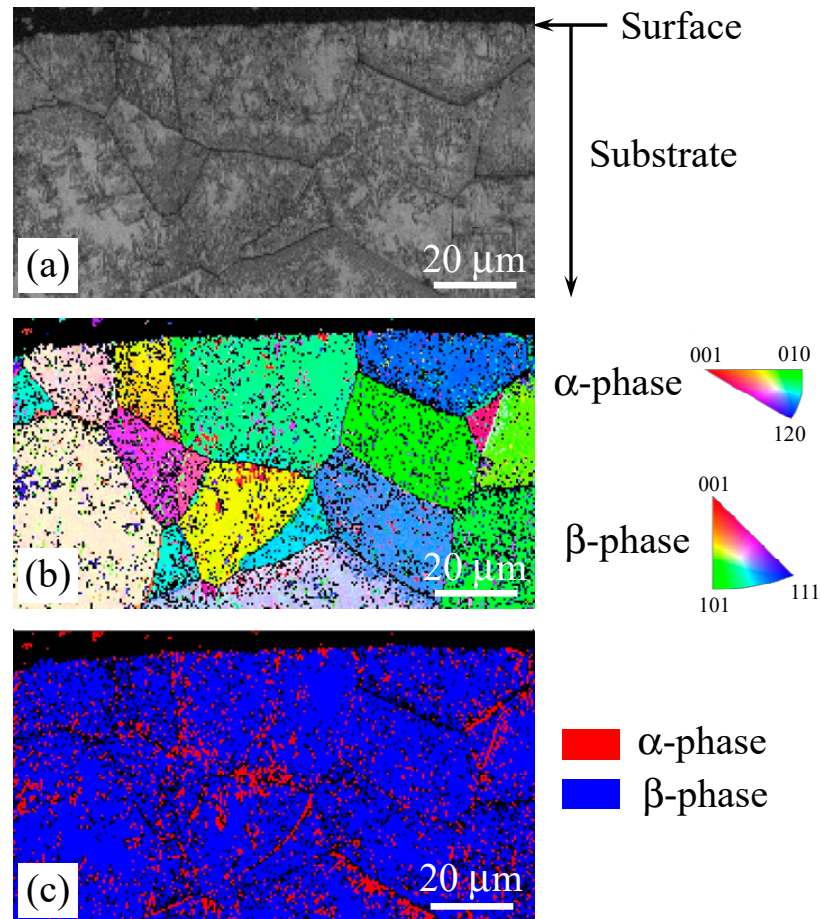


Figure 6. EBSD analysis for cross section of FPP-treated specimen: (a) image quality (IQ) map; (b) IPF map; (c) phase map.

3.3. Hardness and Residual Stress Measurements on the FPP-Treated Ti-22V-4Al Alloy

Figure 7 shows the distribution of Vickers hardness at various cross-sectional depths for the FPP-treated specimen. The hardness on the surface of the FPP-treated specimen was 453 HV. Compared with the substrate (261 ± 2.9 HV), the surface became 73% harder. The interior hardness of the FPP-treated specimen decreased with increasing depth and corresponded to that of the untreated specimen at a depth of 30 μm . In other words, the thickness of the work-hardened layer formed by FPP was approximately 30 μm .

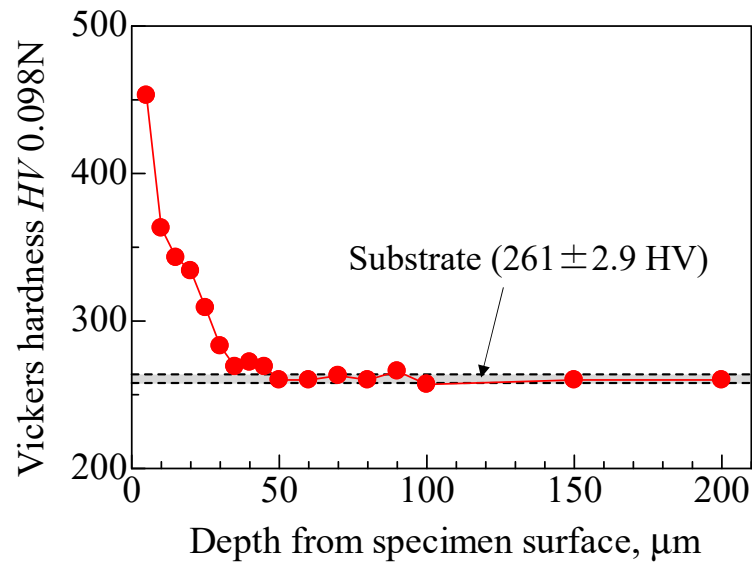


Figure 7. Distribution of Vickers hardness at various cross-sectional depths for FPP-treated specimen.

Figure 8 shows the distribution of the residual stress and the XRD FWHM at various cross-sectional depths for the FPP-treated specimen. As shown in Figure 8a, the compressive residual stress on the surface of the untreated specimen was 306 MPa. This residual stress was caused by buff finishing. The thickness of the surface layer, at which compressive residual stress was generated, was approximately 50 μm . As a result of the comparison of the FWHM profile (Figure 8b) and the Vickers hardness profile (Figure 7), it is clear that both profiles show a very similar behavior. It is well known that FWHM values are useful means to characterize the degree of work hardening, since they usually correlate well with the hardness in soft and medium-hard mechanically surface-treated materials [26]. Therefore, it is confirmed that the depth of work hardening was approximately 50 μm .

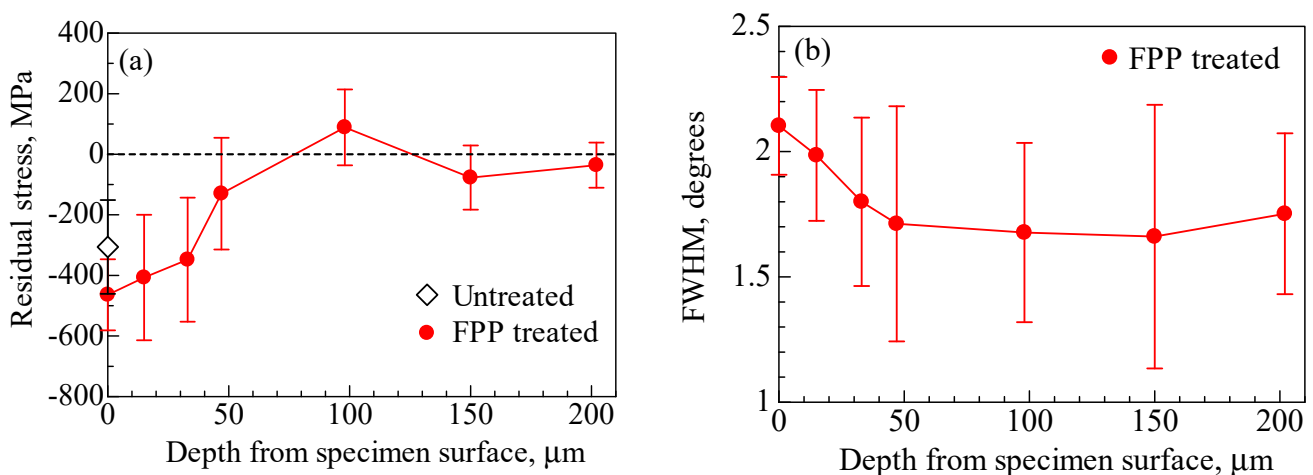


Figure 8. (a) Residual stress and (b) FWHM values as a function of depth into the surface of FPP-treated specimen.

3.4. Fatigue Properties of the FPP-Treated Ti-22V-4Al Alloy

Figure 9 shows the results of the rotating fatigue tests for the untreated and the FPP-treated specimens. In this figure, data points with an arrow indicate the run-out of the specimen, which was not failed until the number of stress cycles was 10^9 . In each specimen, a fatigue limit was not clearly observed so that the $S-N$ curve was determined based on the curve of the $S-N$ model in the JSMS standard regression models [27]. Regression $S-N$

curves for the untreated and FPP-treated specimens are respectively expressed by the following formulae:

$$\text{Untreated : } \sigma_a = 10^{(-0.80825 \log(N) + 5.7133)} + 505.30 \quad (2)$$

$$\text{FPP-treated : } \sigma_a = 10^{(-0.50499 \log(N) + 4.1259)} + 591.95 \quad (3)$$

where σ_a is the stress amplitude applied to the specimen surface (MPa), and N is the number of cycles.

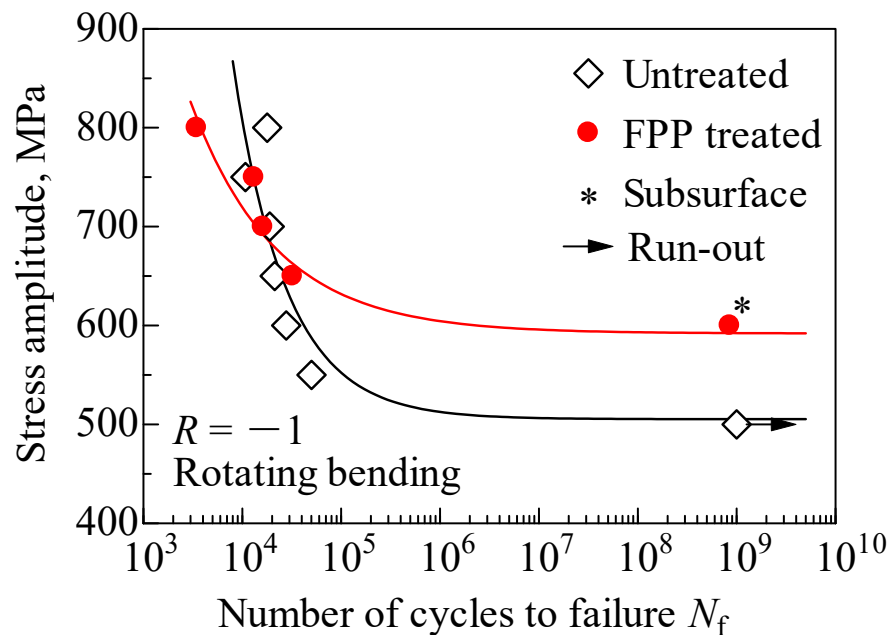


Figure 9. S–N diagram for untreated and FPP-treated specimens.

At high stress levels greater than 700 MPa, there is no improvement in fatigue life by FPP; nevertheless, a work-hardened layer and high compressive residual stress were generated at the specimen surface. As shown in Figure 3, SEM observation of the FPP-treated specimen surface indicated the rough surface formed by FPP. It is suggested that the asperity formed on the specimen surface can be a crack starter and deteriorate the fatigue life. On the other hand, at low stress levels lower than 700 MPa, the fatigue life of the FPP-treated specimen was longer than that of the untreated specimen. The FPP-treated specimen failed at $\sigma_a = 600$ MPa, the fatigue life was $N_f = 1.0 \times 10^9$ cycles, and the subsurface fracture mode was observed. In shot-peened specimens, fatigue crack initiated from the surface of the specimen at a high stress level, while at a low stress level, fatigue crack initiated from the subsurface [28,29]. The same phenomenon is assumed to have occurred in the FPP-treated specimen. Furthermore, if more fatigue tests are performed for the FPP-treated specimen, the duplex S–N characteristics [30] may appear.

The fracture surfaces of all failed specimens were examined using SEM to determine the fatigue fracture mechanism. Figure 10 shows the SEM micrographs of the crack initiation site in each specimen failing at high and low stress levels. At a high stress level ($\sigma_a = 800$ MPa), a fatigue crack was initiated at the specimen surface in the untreated specimen. No defect was found at the crack initiation site, and the fatigue crack was caused by crystal grain slip. On the other hand, in the case of the FPP-treated specimen, a defect was found at the crack initiation site, and it was formed by the collision of HAp shot particles with the specimen surface during the process of FPP. Therefore, the reason the fatigue strength was not improved was that even though a work-hardened layer was generated, the high compressive residual stress caused the formation of defects during the FPP process, and they became crack starters. At a low stress level ($\sigma_a = 600$ MPa), in

the untreated specimen, a fatigue crack was initiated at the specimen surface, the same as when the specimen failed at a high stress level. In the case of the FPP-treated specimen that failed at a low stress level of 600 MPa, it seems that the crack initiated below the specimen surface. Thus, the subsurface-initiated fracture mode occurred in this case. However, no defect (inclusion or defect) was found at the crack initiation site.

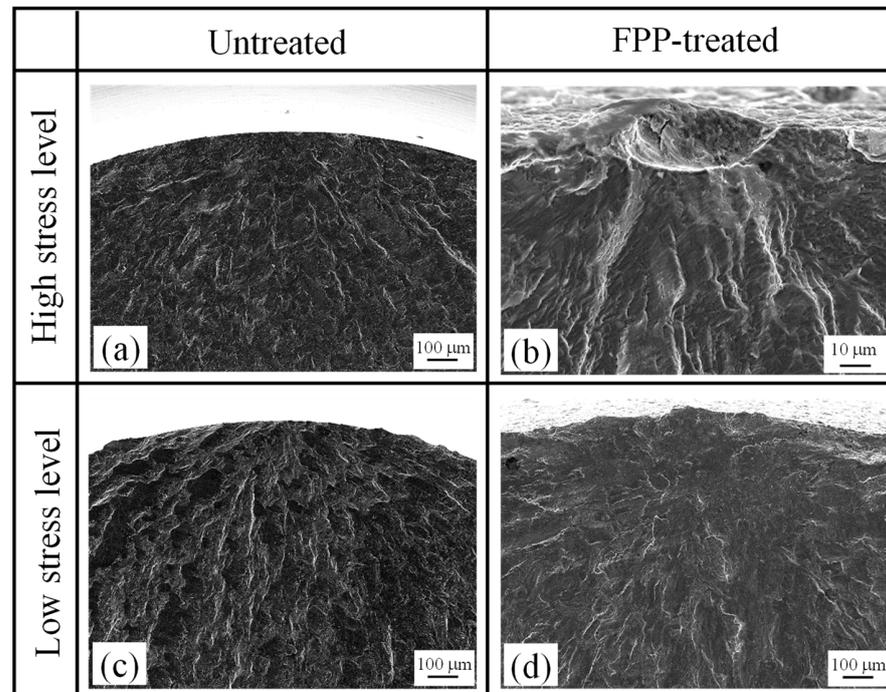


Figure 10. SEM micrographs showing crack initiation site of untreated specimen and FPP-treated specimen failing at (a,b) high ($\sigma_a = 800$ MPa) and (c,d) low ($\sigma_a = 600$ MPa) stress levels.

As can be seen in Figure 10, the FPP-treated specimens showed different failure modes at high and low stress levels. Figure 11 shows a schematic illustration of the fracture mechanism for the FPP-treated specimen. Figure 11a indicates a crack initiated at the surface of the substrate (surface-initiated fracture), and Figure 11b indicates a crack initiated below the surface of the substrate (subsurface-initiated fracture). As shown in Figures 7 and 8, based on the results of Vickers hardness and residual stress measurements, the thickness of the work-hardened layer and the depth of compressive residual stress were approximately 30 μm . Therefore, the resistance to crack initiation became high near the specimen surface, and the crack initiated below the specimen surface. Consequently, the fatigue crack was initiated below the surface of the substrate at a low stress level.

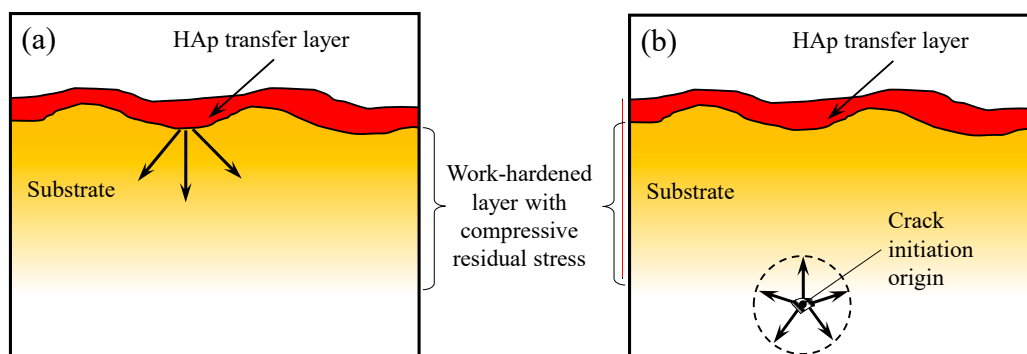


Figure 11. Schematic illustration of fracture mechanism for FPP-treated specimen failed at (a) high and (b) low stress levels.

4. Conclusions

Fine particle peening (FPP) using hydroxyapatite (HAp) shot particles was performed to improve the fatigue strength and form a HAp transfer layer on a beta titanium alloy (Ti–22V–4Al). Rotating bending fatigue tests were performed to investigate the effect of FPP on the fatigue properties. The results obtained are summarized as follows:

1. FPP using HAp shot particles can form a HAp layer on the surface of the Ti–22V–4Al alloy.

2. FPP using HAp shot particles increases the fatigue strength at 10^7 cycles and the fatigue life of the Ti–22V–4Al alloy due to the formation of a work-hardened layer with compressive residual stress on the surface of the Ti–22V–4Al alloy.

3. There is no improvement of fatigue life by FPP at high stress levels greater than 700 MPa, whereas at low stress levels lower than 700 MPa, the fatigue life of FPP-treated specimens was improved by FPP. This is due to work hardening and generation of high compressive residual stress by FPP.

4. The fracture mode of FPP-treated specimens shifted from surface-initiated fracture to subsurface-initiated fracture at a stress level of 600 MPa. FPP-treated specimens showed different failure modes at high and low stress levels.

Author Contributions: Conceptualization and methodology, Y.N. and S.K.; formal analysis, Y.N.; investigation, Y.N., K.N. and T.S.; resources, T.A.; writing—original draft preparation, Y.N.; writing—review and editing, K.N., T.A., T.S. and S.K.; supervision, Y.N. and S.K.; funding acquisition, Y.N. All authors have read and agreed to the published version of the manuscript.

Funding: This research was funded by the Japan Society for the Promotion of Science, Japan, grant number 16K17986, and the Naito Science and Engineering Foundation.

Institutional Review Board Statement: Not applicable.

Informed Consent Statement: Not applicable.

Data Availability Statement: Not applicable.

Acknowledgments: The beta titanium alloy (Ti–22V–4Al) used in this research was supplied by Daido Steel Co., Ltd. FPP treatment was conducted on the basis of the Japanese patent (No. 3314070) applied by Fuji Kihan Co., Ltd., and the Aichi Center for Industry and Science Technology.

Conflicts of Interest: The authors declare no conflict of interest.

References

1. Long, M.; Rack, H.J. Titanium alloys in total joint replacement—a materials science perspective. *Biomaterials* **1998**, *19*, 1621–1639. [[CrossRef](#)]
2. McEvily, A.J.; Nakamura, T.; Oguma, H.; Yamashita, K.; Matsunaga, H.; Endo, M. On the mechanism of very high cycle fatigue in Ti–6Al–4V. *Scr. Mater.* **2008**, *59*, 1207–1209. [[CrossRef](#)]
3. Günther, J.; Krewerth, D.; Lippmann, T.; Leuders, S.; Tröster, T.; Weidner, A.; Biermann, H.; Niendorf, T. Fatigue life of additively manufactured Ti–6Al–4V in the very high cycle fatigue regime. *Int. J. Fatigue* **2017**, *94*, 236–245. [[CrossRef](#)]
4. Cao, F.; Chandran, K.S.R. The role of crack origin size and early stage crack growth on high cycle fatigue of powder metallurgy Ti–6Al–4V alloy. *Int. J. Fatigue* **2017**, *102*, 48–58. [[CrossRef](#)]
5. Yang, K.; He, C.; Huang, Q.; Huang, Z.Y.; Wang, C.; Wang, Q.; Liu, Y.J.; Zhong, B. Very high cycle fatigue behaviors of a turbine engine blade alloy at various stress ratios. *Int. J. Fatigue* **2017**, *99*, 35–43. [[CrossRef](#)]
6. Huang, Z.Y.; Liu, H.Q.; Wang, H.M.; Wagner, D.; Khan, M.K.; Wang, Q.Y. Effect of stress ratio on VHCF behavior for a compressor blade titanium alloy. *Int. J. Fatigue* **2016**, *93*, 232–237. [[CrossRef](#)]
7. Nikitin, A.; Palin-Luc, T.; Shanyavskiy, A. Crack initiation in VHCF regime on forged titanium alloy under tensile and torsion loading modes. *Int. J. Fatigue* **2016**, *93*, 318–325. [[CrossRef](#)]
8. Yang, Y.; Chang, E. Measurements of residual stresses in plasma-sprayed hydroxyapatite coatings on titanium alloy. *Surf. Coat. Technol.* **2005**, *190*, 122–131. [[CrossRef](#)]
9. Li, H.; Khor, K.A.; Cheang, P. Adhesive and bending failure of thermal sprayed hydroxyapatite coatings: Effect of nanostructures at interface and crack propagation phenomenon during bending. *Eng. Fract. Mech.* **2007**, *74*, 1894–1903. [[CrossRef](#)]
10. Nimkerdphol, A.R.; Otsuka, Y.; Mutoh, Y. Effect of dissolution/precipitation on the residual stress redistribution of plasma-sprayed hydroxyapatite coating on titanium substrate in simulated body fluid (SBF). *J. Mech. Behav. Biomed. Mater.* **2014**, *36*, 98–108. [[CrossRef](#)]

11. Laonapakul, T.; Nimkerdphol, A.R.; Otsuka, Y.; Mutoh, Y. Failure behavior of plasma-sprayed HAp coating on commercially pure titanium substrate in simulated body fluid (SBF) under bending load. *J. Mech. Behav. Biomed. Mater.* **2012**, *15*, 153–166. [[CrossRef](#)] [[PubMed](#)]
12. Reis, R.L.; Monteiro, F.J. Crystallinity and structural changes in HA plasma-sprayed coatings induced by cyclic loading in physiological media. *J. Mater. Sci. Mater. Med.* **1996**, *7*, 407–411. [[CrossRef](#)]
13. Gariboldi, E.; Previtali, B. High tolerance plasma arc cutting of commercially pure titanium. *J. Mater. Process. Technol.* **2005**, *160*, 77–89. [[CrossRef](#)]
14. Kameyama, Y.; Ohmori, H.; Kasuga, H.; Kato, T. Fabrication of micro-textured and plateau-processed functional surface by angled fine particle peening followed by precision grinding. *CIRP Ann. Manuf. Technol.* **2015**, *64*, 549–552. [[CrossRef](#)]
15. Kameyama, Y.; Komotori, J. Effect of micro ploughing during fine particle peening process on the microstructure of metallic materials. *J. Mater. Process. Technol.* **2009**, *209*, 6146–6155. [[CrossRef](#)]
16. Kameyama, Y.; Komotori, J. Tribological properties of structural steel modified by fine particle bombardment (FPB) and diamond-like carbon hybrid surface treatment. *Wear* **2007**, *263*, 1354–1363. [[CrossRef](#)]
17. Kameyama, Y.; Nishimura, K.; Sato, H.; Shimpo, R. Effect of fine particle peening using carbon-black/steel hybridized particles on tribological properties of stainless steel. *Tribol. Int.* **2014**, *78*, 115–124. [[CrossRef](#)]
18. Kikuchi, S.; Yoshida, S.; Nakamura, Y.; Nambu, K.; Akahori, T. Characterization of the hydroxyapatite layer formed by fine hydroxyapatite particle peening and its effect on the fatigue properties of commercially pure titanium under four-point bending. *Surf. Coat. Technol.* **2016**, *288*, 196–202. [[CrossRef](#)]
19. Kikuchi, S.; Nakamura, Y.; Nambu, K.; Akahori, T. Formation of the hydroxyapatite layer on Ti-6Al-4V ELI alloy by fine particle peening. *Int. J. Autom. Technol.* **2017**, *11*, 915–924. [[CrossRef](#)]
20. Kikuchi, S.; Nakamura, Y.; Nambu, K.; Akahori, T. Formation of a hydroxyapatite layer on Ti-29Nb-13Ta-4.6Zr and enhancement of four-point bending fatigue characteristics by fine particle peening. *Int. J. Lightweight Mater. Manuf.* **2019**, *2*, 227–234. [[CrossRef](#)]
21. Kikuchi, S.; Nakamura, Y.; Nambu, K.; Ando, M. Effect of shot peening using ultra-fine particles on fatigue properties of 5056 aluminum alloy under rotating bending. *Mater. Sci. Eng. A* **2016**, *652*, 279–286. [[CrossRef](#)]
22. Oguri, K. Fatigue life enhancement of aluminum alloy for aircraft by fine particle shot peening (FPSP). *J. Mater. Process. Technol.* **2011**, *211*, 1395–1399. [[CrossRef](#)]
23. Kikuchi, S.; Nakahara, Y.; Komotori, J. Fatigue properties of gas nitride austenitic stainless steel pre-treated with fine particle peening. *Int. J. Fatigue* **2010**, *32*, 403–410. [[CrossRef](#)]
24. Morita, T.; Noda, S.; Kagaya, C. Influence of hardness of substrates on properties of surface layer formed by fine particle bombarding. *Mater. Sci. Eng. A* **2013**, *574*, 197–204. [[CrossRef](#)]
25. Sakai, T.; Furusawa, T.; Takizawa, R.; Oguma, N.; Hohjo, H.; Ikuno, H. Development of multi-type high frequency fatigue testing machines in rotating bending and axial loading. In Proceedings of the Hael Mughrabi Honorary Symposium, New Orleans, LA, USA, 9–13 March 2008; pp. 241–246.
26. Nalla, R.K.; Altenberger, I.; Noster, U.; Liu, G.Y.; Scholtes, B.; Ritchie, R.O. On the influence of mechanical surface treatments deep rolling and laser shock peening on the fatigue behavior of Ti-6Al-4V at ambient and elevated temperature. *Mater. Sci. Eng. A* **2003**, *355*, 216–230. [[CrossRef](#)]
27. Sakai, T.; Sugeta, A. Publication of the second edition of “Standard evaluation method of fatigue reliability for metallic materials” [Standard regression method of S-N curves]. *J. Soc. Mater. Jpn.* **2005**, *54*, 37–43. [[CrossRef](#)]
28. Zhang, J.; Li, X.; Yang, B.; Wang, H.; Zhang, J. Effect of micro-shot peening on fatigue properties of precipitate strengthened Cu-Ni-Si alloy in air and in salt atmosphere. *Surf. Coat. Technol.* **2019**, *359*, 16–23. [[CrossRef](#)]
29. Benedetti, M.; Fontanari, V.; Bandini, M.; Savio, E. High- and very high-cycle plain fatigue resistance of shot peened high-strength aluminum alloys: The role of surface morphology. *Int. J. Fatigue* **2015**, *70*, 451–462. [[CrossRef](#)]
30. Sakai, T.; Lian, B.; Takeda, M.; Shiozawa, K.; Oguma, N.; Ochi, Y.; Nakajima, M.; Nakamura, T. Statistical duplex S-N characteristics of high carbon chromium bearing steel in rotating bending in very high cycle regime. *Int. J. Fatigue* **2010**, *32*, 497–504. [[CrossRef](#)]